# A heat transfer - friction analogy for fluids at supercritical pressure

Peeters, J. W.R.; Rohde, M.

**DOI**
10.1016/j.supflu.2019.03.009

**Publication date**
2019

**Document Version**
Accepted author manuscript

**Published in**
Journal of Supercritical Fluids

# A heat transfer - friction analogy for fluids at supercritical pressure

J. W. R. Peeters[a,*], M. Rohde[b]

[a] *Process and Energy, Mechanical, Maritime and Materials Engineering, Delft University of Technology*
[b] *Reactor Physics and Nuclear Materials, Applied Sciences, Delft University of Technology*

## Abstract

A new friction-heat transfer analogy for the prediction of heat transfer to turbulent fluids at supercritical pressure is presented. This analogy is based on the observation that the predominent events that determine the turbulent heat flux known as hot ejections and cold sweeps have different thermophysical properties. This observation is used to derive a new friction-heat transfer analogy, which we call the ejection-sweep analogy. It is shown that the ejection-sweep analogy yields very good results with respect to predicting heat transfer coefficients for different fluids (water, $CO_2$, Helium, R22 and R134a) that are heated at supercritical pressure at low heat flux to mass flux ratios. Furthermore, the new analogy performs much better than the Chilton-Colburn analogy. The new analogy was also compared with two well-known relations from literature. It was found that the ejection-sweep analogy predictions are more consistent with respect to the investigated fluids than the relations from literature and that the analogy can be applied to at least all fluids studied in this work. The ejection-sweep analogy can be used in the development of more advanced heat transfer models that include buoyancy and acceleration effects.

## List of Symbols

### Acronyms

CC Chilton-Colburn

ES Ejection-Sweep

*Corresponding author
*Email address:* j.w.r.peeters@tudelft.nl (J. W. R. Peeters)

**Greek Symbols**

| | |
|---|---|
| $\alpha_{(...)}$ | area fraction $\left(= \frac{A_{(...)}}{A}\right)$ |
| $\epsilon$ | constant of proportionality $\left(= \frac{\phi_l}{G}\right)$ |
| $\eta$ | non-dimensional radius $\left(= \frac{\xi}{\xi_{(...),0}}\right)$ |
| $\gamma$ | ratio of time scales $(= t_{burst}/t)$ |
| $\lambda$ | thermal conductivity, W/m/K |
| $\mu$ | dynamic viscosity, Pa s |
| $\nu$ | kinematic viscosity, $m^2/s$ |
| $\phi$ | mass flux of an ejection/sweep, $kg/m^2/s$ |
| $\rho$ | density, $kg/m^3$ |
| $\tau$ | shear stress, Pa |
| $\xi$ | radial coordinate (inside ejection/sweep), m |
| $\xi_{(...),0}$ | radius of the ejection (h)/sweep (c), m |

**Roman Symbols**

| | |
|---|---|
| $\Delta h$ | enthalpy difference between ejection/sweep and bulk, J |
| $\Delta T$ | temperature difference between ejection/sweep and bulk, K |
| $\mathcal{F}$ | function of thermophysical property ratios |
| $\mathcal{G}$ | function of non-dimensional groups |
| $\overline{T}$ | mean temperature of ejection/sweep, K |
| $A$ | cross-sectional area of the burst, $m^2$ |
| $b, b_2$ | model constants |
| $c_h, c_c$ | model constants |
| $c_p$ | specific heat capacity, J/kg/K |
| $D_h$ | hydraulic diameter, m |

$f_{\Delta h}$ non-dimensional enthalpy difference $\left(= \frac{\Delta h}{h_w - h_b}\right)$

$f_{\phi_{(...)}}$ non-dimensional mass flux $\left(= \frac{\phi_{(...)}}{\phi_{(...),l}}\right)$

$G$ mass flux in the mean flow direction, kg/m$^2$/s

$HTC$ heat transfer coefficient $= \left(\frac{q}{T_w - T_b}\right)$, W/m$^2$/K

$I$ integrated function

$p$ pressure, Pa

$p_r$ reduced pressure

$Q$ heat transferred, J

$q$ heat flux, W/m$^2$

$T$ temperature, K

$t$ duration, s

$U$ velocity, m/s

$u_\tau$ friction velocity $= \left(\sqrt{\tau/\rho}\right)$, m/s

**Superscripts**

$+$ scaled with viscous units

$n, m, p$ powers

**Subscripts**

$ac$ acceleration

$b$ bulk

$burst$ bursting phase

$c$ cold sweep

$cond$ conduction

$h$ hot ejection

$in$ inlet

$iso$ isothermal

$l$ centreline of the ejection/sweep

$pc$ pseudo-critical

$qs$ quiescent

$tot$ total

$w$ wall

**Non-dimensional numbers**

$\overline{Pr}$ alternate Prandtl number $\left(= \frac{\mu_b}{\lambda_b}\frac{h_w - h_b}{T_w - T_b}\right)$

$C_f$ skin friction coefficient $\left(= \frac{2\tau}{\rho_b U_b^2}\right)$

$Nu$ Nusselt number $\left(= \frac{HTC \times D_h}{\lambda}\right)$

$Pr$ Prandtl number $= \left(\frac{\mu c_p}{\lambda}\right)$

$Re$ Reynolds number $\left(= \frac{GD_h}{\mu_b}\right)$

## 1. Introduction

When a supercritical fluid is isobarically heated, its thermophysical properties change sharply. Due to the strong thermophysical properties' variations, heat transfer to turbulent fluids is difficult to predict, as Nusselt number relations developed for fluids at sub-critical pressure fail to predict heat transfer at supercritical pressure accurately. In the past, researchers have focused primarily on the effect of streamwise flow acceleration due to thermal expansion and/or buoyancy (both of which are the result of density variations) [8], [28]. The effect of variable heat capacity, thermal conductivity and molecular Prandtl number have been used in Nusselt number relations for heat transfer to supercritical fluids before by using dimensional analysis. However, such relations often lack physical insight.

It is clear from literature that an accurate relation for the prediction of heat transfer to fluids at supercritical pressure is still sought after. Recent efforts include a two-layer model [17], a heat transfer model that includes time-averaged estimates of average thermophysical

properties from probability density functions [14], a predictive-corrective approach [15], but also physically-based semi-empirical models of buoyancy-influenced and inertia-influenced heat transfer [9].

In this paper, we present a new heat transfer model, which is based on our observations of direct numerical simulations of heated turbulent flows at supercritical fluids [18]. This model takes variable thermal conductivity, and specific heat capacity into account. In the next section, we will first show the model concept, after which we will derive a general form for a Nusselt number relation. Subsequently, the model is cast into a useable form, after which we will show comparisons with experimental results. Finally, we will summarize our conclusions.

## 2. The model

### *2.1. Concept*

On a rather simplistic level, wall bounded turbulent flows can be regarded to be locally either in a quiescent state (i.e. small momentum variations) or a bursting state (locally large momentum variations). For the model, it is assumed that the quiescent state has a duration $t_{qs}$, while the bursting phase has a duration $t_{burst}$. During the bursting phase, hot fluid moves away from a heated surface, while cold fluid moves towards it. These motions will be referred to as hot ejections and cold sweeps. The total time during which heat transfer takes place is denoted as $t_{tot} \equiv t_{qs} + t_{burst}$, where $t_{burst}$ is the time during which the hot ejection and cold sweep occur. In reality, hot ejections and cold sweep have complicated shapes. Following Hetsroni et al. [4], the hot ejection is modelled as an axisymmetric jet. The effect of the cold sweep is considered here as well and is likewise modelled. Figure 1 shows the concept of a hot ejection and a cold sweep that occur in a flow near a heated surface. The mass flux of the mean flow is defined as $G$. The hot ejection is assumed to have a cross-sectional area of $A_h$ and a wall normal mass flux $\phi_h$ with a corresponding radius of $\xi_{h,0}$, while the cold sweep is assumed to have an area of $A_c$ and a wall normal mass flux $\phi_c$ with a radius of $\xi_{c,0}$. The burst phase is assumed to constitute both the hot ejection and the cold sweep. The burst has therefore an cross-sectional area $A = A_h + A_c$. Both the hot ejection and the cold sweep

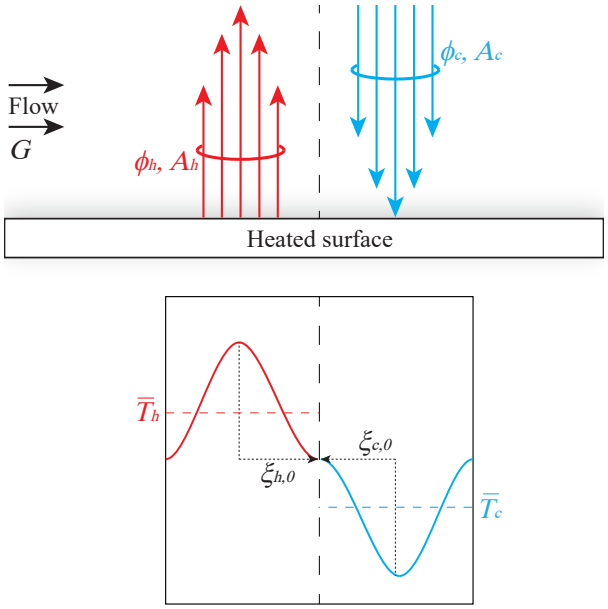


Figure 1: The model concept. The hot ejection has a different mass flux $\phi_h$ and cross-sectional area $A_h = \pi\xi_{h,0}^2$ than the cold sweep $\phi_c$ and $A_c = \pi\xi_{c,0}^2$.

have a temperature distribution, as is indicated by the coloured curves in figure 1. The mean temperatures of the hot ejection and cold burst are denoted as $\overline{T_h}$ and $\overline{T_c}$.

### *2.2. Derivation*

The derivation that was presented by Hetsroni et al. [4] is followed here, except for the fact that the cold sweep is included and that the hot ejection and cold sweep have different thermophysical properties. The total heat that is transferred during the quiescent and the turbulent phases is written as $Q_{tot}$ and is split into a contribution by conduction $Q_{cond}$ and a contribution from turbulence:

$$Q_{tot} = \overbrace{Q_{cond}}^{\text{laminar}} + \underbrace{Q_h + Q_c}_{\text{turbulence}}, \tag{1}$$

in which the turbulence contribution is split into a contribution by the hot ejection $Q_h$ and the cold sweep $Q_c$. The total heat transferred during time $t_{tot}$ can be modelled as:

$$Q_{tot} = HTC(T_w - T_b) \times A \times t_{tot}, \tag{2}$$

where $HTC$ is the heat transfer coefficient, $T_w$ the wall temperature, $T_b$ the bulk temperature. The conduction part is written as

$$Q_{cond} = q_{cond} \times A \times t_{qs}, \tag{3}$$

where $q_{cond}$ is the conductive heat flux. The next step is to rewrite the turbulent parts of equation (1). $Q_h$ is modelled as an axially symmetrical jet, with a radius $\xi_{h,0}$. The total energy that is transported from the wall is then

$$Q_h = 2\pi \int_0^{\xi_{h,0}} \phi_h \Delta h \xi d\xi \times t_{burst} \tag{4}$$

Here, $\Delta h$ is the enthalpy difference between that of the fluid moving away from the wall ($h$) and that of the bulk region of the fluid ($h_b$). $\phi_h$ is the wall normal mass flux of the hot ejection. The enthalpy difference corresponds to a temperature difference $\Delta T = T - T_b$. Defining the non-dimensional radius $\eta \equiv \xi/\xi_{h,0}$ yields for the hot part:

$$Q_h = 2\pi\xi_{h,0}^2 \int_0^1 \phi_h \Delta h \eta d\eta \times t_{burst} \tag{5}$$

Hetsroni et al. [4] assume that the velocity profile is simply a function of $\eta$ and that the temperature difference is a function of $\eta$ and the Prandtl number $Pr$, based on experimental results Abramovich [1]. Similarly, it is assumed here that,

$$\frac{\Delta h}{h_w - h_b} \equiv f_{\Delta h}(\eta, Pr_h) \quad \text{and} \quad \frac{\phi_h}{\phi_{h,l}} \equiv f_{\phi_h}(\eta) \tag{6}$$

where $\phi_{h,l}$ represents the centreline mass flux value of the hot ejection , $h_w$ represents the enthalpy at the wall and where $f_{\Delta h}$ and $f_{\phi_h}$ are functions representing the non-dimensional enthalpy difference and mass flux, respectively. Note that the Prandtl number has an index 'h', meaning that the enthalpy profile depends on local material properties. Equation (6) can now be used to rewrite equation (5) into:

$$Q_h = 2\pi\xi_{h,0}^2 \phi_{h,l}(h_w - h_b) \underbrace{\int_0^1 f_{\Delta h}(\eta, Pr_h) f_{\phi_h}(\eta)\eta d\eta}_{I(Pr_h)} \times t_{burst} \tag{7}$$

Making similar assumptions as before for the cold sweep,

$$\frac{\Delta h}{h_w - h_b} = f_{\Delta h}(\eta, Pr_c), \quad \text{and} \quad \frac{\phi_c}{\phi_{c,l}} = f_{\phi_c}(\eta), \tag{8}$$

where $\phi_{c,l}$ is the centreline mass flux value of the cold sweep, yields;

$$Q_c = 2\pi\xi_{c,0}^2\phi_{c,l}(h_w - h_b)\underbrace{\int_0^1 f_{\Delta h}(\eta, Pr_c)f_{\phi_c}(\eta)\eta d\eta}_{I(Pr_c)} \times t_{burst} \tag{9}$$

The result of equations (7) and (9) is that the hot fluid depends on $Pr_h = Pr(\overline{T_h})$, while the cold part of the fluid depends on $Pr_c = Pr(\overline{T_c})$. Combining equations (1), (2), (3),(7) and (9) results in

$$\begin{aligned} HTC(T_w - T_b) \times A \times t_{tot} &= q_{cond} \times A \times t_{qs} \\ &+ 2\phi_{h,l}(h_w - h_b)I(Pr_h) \times \pi\xi_{h,0}^2 \times t_{burst} \\ &+ 2\phi_{c,l}(h_w - h_b)I(Pr_c) \times \pi\xi_{c,0}^2 \times t_{burst} \end{aligned} \tag{10}$$

Multiplying the left and right side of equation (10) with a characteristic length scale $D_h$ and dividing by the bulk thermal conductivity $\lambda_b$, $T_w - T_b$, $A$ and $t_{tot}$ gives:

$$\begin{aligned} Nu_b = \frac{HTC \times D_h}{\lambda_b} &= \frac{q_{cond}D_h}{\lambda_b(T_w - T_b)} \times \alpha_{qs} \\ &+ 2\left(\frac{\phi_{h,l}(h_w - h_b)D_h}{\lambda_b(T_w - T_b)}\right) I(Pr_h) \times \alpha_h \times \gamma \\ &+ 2\left(\frac{\phi_{c,l}(h_w - h_b D_h}{\lambda_b(T_w - T_b)}\right) I(Pr_c) \times \alpha_c \times \gamma \end{aligned} \tag{11}$$

The fractions, denoted with $\alpha_{(...)}$ and $\gamma$ are defined as follows: $\alpha_{qs} \equiv t_{qs}/t_{tot}$, $\alpha_c \equiv \pi\xi_{c,0}^2/A$, $\alpha_h \equiv \pi\xi_{h,0}^2/A$, $\gamma \equiv t_{burst}/t_{tot}$. The relation between the time constants is $1 = \alpha_{t_{qs}} + \gamma$. The burst duration is much smaller than the duration of the quiescent phase. Thus, it follows that $1 - \gamma \approx 1$ for $\gamma << 1$. Defining $Nu_{cond} \equiv q_{cond}D_h/\lambda_b(T_w - T_b)$, $Re_b = GD_h/\mu_b$ and $\overline{Pr} = \mu_b(h_w - h_b)/(\lambda_b(T_w - T_b))$, yields;

$$\begin{aligned} Nu_b &= Nu_{cond} \\ &+ 2\left(\frac{\phi_{h,l}}{G}\right) Re_b\overline{Pr}I(Pr_h) \times \alpha_h \times \gamma \\ &+ 2\left(\frac{\phi_{c,l}}{G}\right) Re_b\overline{Pr}I(Pr_c) \times \alpha_c \times \gamma \end{aligned} \tag{12}$$

Equation (12) represents a general form of a Nusselt relation that could be used to describe heat transfer to fluids with variable thermophysical properties.

*2.3. Creating a relation*

Equation (12) is not ready to be used as a heat transfer model, since the parameters $Nu_{cond}$, $\phi_{h,l}/G$, $\phi_{c,l}/G$, $I(Pr_w)$, $I(Pr_c)$, as well as the fractions $\alpha_h$, $\alpha_c$ and $\gamma$ need to be modelled. A model for the wall-normal motions is sought first. We assume that the magnitude of the wall normal mass fluxes in the centre of the ejections and sweeps can be modelled as $\phi_{h,l} = \phi_{c,l} = \epsilon G$, with $\epsilon < 1$, where $G$ (kg/m$^2$s) is the mean streamwise mass flux. Furthermore, the time- and surface fractions need to be modelled. Hetsroni et al. [4] uses experimental observations, see for instance [2], to estimate the burst duration. Their reasoning is as follows: the duration of the quiescent phase scaled with wall units is approximately constant, or $t^+_{tot} \equiv t_{tot}(u^2_\tau/\nu) = 91.5$, where the friction velocity $u_\tau \equiv \sqrt{\tau_w/\rho}$. $t_{burst}$ is modelled as $t_{burst} = b\nu/U_b^2$, where $U_b = G/\rho$ and $b$ is a model constant. This model yields $\gamma = t_{burst}/t_{tot} = b_2(u_\tau/U_b)^2$, where $b_2 = b/91.5$. In an isothermal flow, $u_\tau$ can be estimated from a skin friction correlation, so that $\gamma = b_2 C_f/2$. We make an 'ad hoc' assumption here that in a non-isothermal flow with variable thermophysical properties the same time ratio $\gamma \approx b_2 C_f/2$ holds. Combining this result with $\phi_{h,l} = \phi_{c,l} = \epsilon G$ and with equation (12), yields:

$$\begin{aligned} Nu_b &= Nu_{cond} \\ &+ (2\epsilon \times \alpha_{A_h} \times b_2)\,\frac{C_f}{2} Re_b \overline{Pr} I(Pr_h) \\ &+ (2\epsilon \times \alpha_{A_c} \times b_2)\,\frac{C_f}{2} Re_b \overline{Pr} I(Pr_c) \end{aligned} \tag{13}$$

If the skin friction coefficient reduces to its value under (near) isothermal conditions, it may be possible to construct a relation that reverts to the Chilton–Colburn analogy for constant thermophysical properties, which may be written as:

$$Nu_b = \frac{C_f}{2} Re_b Pr_b^{1/3}. \tag{14}$$

Hetsroni et al. [4] estimate the integral $I(Pr)$ by using explicit functions of the temperature and velocity distributions of the burst. Noting that the integral can be approximated as $I(Pr) \approx APr^n$ and defining that $c_h \equiv 2\epsilon\alpha_{A_h} b_2 A$ and $c_c \equiv 2\epsilon\alpha_{A_c} b_2 A$, results in:

$$Nu_b = Nu_{cond} + \frac{C_f}{2} Re_b \left( c_h \frac{\overline{Pr}}{Pr_h^n} + c_c \frac{\overline{Pr}}{Pr_c^n} \right). \tag{15}$$

Under turbulent conditions, the contribution of $Nu_{cond}$ is negligible. The new relation reverts to the Chilton–Colburn analogy under constant thermophysical property conditions (or near isothermal conditions), i.e. when $\overline{Pr} = Pr_h = Pr_c = Pr$, for $c_c = 1 - c_h$ and $n = 2/3$. This estimate is very close to the numerical result by Hetsroni et al. [4], who reports $n = 0.57$ to 0.8. Thus,

$$Nu_b = \frac{C_f}{2} Re_b \left( c_h \frac{\overline{Pr}}{Pr_h^{2/3}} + c_c \frac{\overline{Pr}}{Pr_c^{2/3}} \right), \tag{16}$$

The factors $\alpha_{A_h}$, $\alpha_{A_c}$, $c_h$ and $c_c$ suggest that the contribution of the hot part to the Nusselt number is different from the contribution by the cold part. In a previous publication, we found evidence that this is indeed the case [18]. Equation (16) depends on $Pr_h \equiv Pr(T_h)$ and $Pr_c \equiv Pr(T_c)$. Keeping in mind that the new analogy should preferably be easy to use, we assume that $Pr_h \approx Pr_w$ and $Pr_c \approx Pr_b$. In order to complete the heat transfer - friction analogy, a slin friction coefficient relation must be known. Furthermore, the constants $c_h$ and $c_c$ must be determined; this will be done by comparing equation (16) with experimental results.

*2.4. Skin friction relations*

Different friction factor relations for heated fluids at supercritical fluids are found in the literature. Many of these relations are the result of an empirical fit of experimental data obtained for a broad range of conditions, i.e. in both deteriorated and normal heat transfer regimes. Friction relations are typically reported in the form:

$$C_f = C_{f,iso} \times \mathcal{F} \left\{ \left( \frac{\rho_b}{\rho_w} \right)^{m_1}, \left( \frac{\mu_b}{\mu_w} \right)^{m_2}, ... \right\}, \tag{17}$$

where $\mathcal{F}$ represents a function of thermophysical property ratios, and $m_1 \neq m_2$. $C_{f,iso}$ can be modelled by the Blasius and the Filonenko relations:

$$C_{f,iso} = \begin{cases} 0.079 Re_b^{-\frac{1}{4}}, & \text{if } Re_b \leq 10^4 \\ \left(1.58 \ln(Re_b) - 3.28\right)^{-2}, & \text{if } Re_b > 10^4. \end{cases} \tag{18}$$

Table 1 shows different friction relations for heated fluids at supercritical pressure. This list is by no means exhaustive and for a review on friction relations for heated fluids, we refer to [21].

Table 1: Friction relations for heated fluids at supercritical pressure

| **source** | $\mathcal{F}(\rho, \mu, ...)$ | **special** |
|---|---|---|
| isothermal | 1.0 | ... |
| Petrov & Popov [19] | $\left(\frac{\mu_w}{\mu_b}\right)^{1/4} + \left(\frac{\rho_w}{\rho_b}\right)^{1/3} \left\lvert\frac{C_{f,ac}}{C_{f,iso}}\right\rvert$ | $C_{f,ac} \equiv \frac{8 q_w \beta_b}{G c_p}$ |
| Tarasova [23] | $\left(\frac{\mu_w}{\mu_b}\right)^{0.22}$ | ... |
| Petukhov [20] | $\left(\frac{\rho_w}{\rho_b}\right)^{0.4}$ | ... |
| Wang [25] | $0.95 \left(\frac{\mu_w}{\mu_b}\right)^{0.56} \left(\frac{\rho_b}{\rho_w}\right)^{0.35} Pr_b^{0.26}$ | annular flows |

### *2.5. Experimental cases*

The experimental cases that were selected to test the developed analogy are listed in table 2. In all of the selected cases, the supercritical fluid was heated. In cooling cases, it is not only difficult to obtain constant wall heat fluxes, but also to obtain the local heat flux [5], [29]. The experiments cover a wide range of experimental parameters, such as the reduced pressure $p_r$ and the hydraulic diameter $D_h$. Furthermore, five different fluids are considered. It is well known that in cases with high heat flux to mass flux ratios, buoyancy and acceleration effects have a profound effect on heat transfer. It is unlikely that a heat transfer - friction analogy will exist under such conditions. Therefore, we have selected only cases with low heat flux to mass flux ratios. We have selected three friction relations. The first friction relation is equation 18. The second and third friction relations are the relations by Petrov and Popov [19] and Tarasova and Leont'ev [23].

Equation (16) was tested against the selected experiments for various combinations of $c_h$ and $c_c$. Reasonable results were found for $c_h \approx 0.7$ and $c_c \approx 0.3$. This result agrees qualitively well with the DNS experiments with regards to the fact that hot outward motions contribute the most to heat transfer. Finally, this results in:

$$Nu_b = \frac{C_f}{2} Re_b \left( 0.7 \frac{\overline{Pr}}{Pr_w^{2/3}} + 0.3 \frac{\overline{Pr}}{Pr_b^{2/3}} \right). \tag{19}$$

The predictions of equation (19) with respect to the heat transfer coefficient are compared to the experimental cases alongside predictions from the Chilton–Colburn relation in the next section.

Table 2: The selected experimental cases.

| **source** | **fluid** | $p_r$ | $q/G$ (kJ/kG) | $D_h$ (mm) | **orientation** |
|---|---|---|---|---|---|
| Yamashita et al. [27] | R22 | 1.10 | 0.025-0.030 | 4.4 - 13 | upward |
| Cui et al. [3] | R134a | 1.06-1.18 | 0.040 | 8.0 | downward |
| Kim et al. [11] | $CO_2$ | 1.10 | 0.042 | 4.4 - 9.0 | upward |
| Kim et al. [10] | $CO_2$ | 1.05 | 0.042 | 4.4 | upward |
| Kurganov et al. [13] | $CO_2$ | 1.22 | 0.05 | 22.7 | upward/ downward |
| Ito et al. [6] | Helium | 1.32-2.20 | 0.0125 | 1.25 | upward/ downward |
| Yamagata et al. [26] | $H_2O$ | 1.11 | 0.13-0.18 | 7.5 | horizontal/ upward/ downward |
| Swenson et al. [22] | $H_2O$ | 1.03-1.41 | 0.36 | 9.042 | upward |
| Mokry et al. [16] | $H_2O$ | 1.09 | 0.28 | 10 | upward |
| Vikhrev et al. [24] | $H_2O$ | 1.20 | 0.5 | 20.4 | upward |
| Krasyakova et al. [12] | $H_2O$ | 1.11 | 0.46 | 20 | downward |

## 3. Results

The performance of equation (19) is demonstrated in three parts. In the first part, we will only consider cases with a high reduced pressure and a low heat flux. In the second part, we will investigate cases with a higher heat flux and/or a lower reduced pressure . In these two parts, we will compare results from the ejection-sweep analogy (abbreviated as *ES*) with results obtained with the Chilton–Colburn analogy (abbreviated as *CC*). In the last part, we will compare the ejection-sweep analogy to results obtained with results that were presented previously in the literature.

### *3.1. High reduced pressure/low heat flux*

In figure 2, we compare both analogies to the selected R22 experiments by Yamashita et al. [27]. In all three cases, the Chilton–Colburn analogy shows a large deviation from the experimental results in the region where $h_b \approx 325 - 375$ kJ/kg. However, it is clear that the ejection-sweep analogy yields excellent results for all three friction relations. The Chilton–Colburn analogy predicts a peak in the heat transfer coefficient when $h_b \approx h_{pc}$, while the ejection-sweep shows a peak at a location where $h_b < h_{pc}$. This is in fact a feature of the

ejection-sweep analogy: for higher heating rates, the peak in heat transfer coefficient shifts towards the start of the heated length, because the ejection-sweep analogy depends on both $Pr_w$ as well as $Pr_b$.

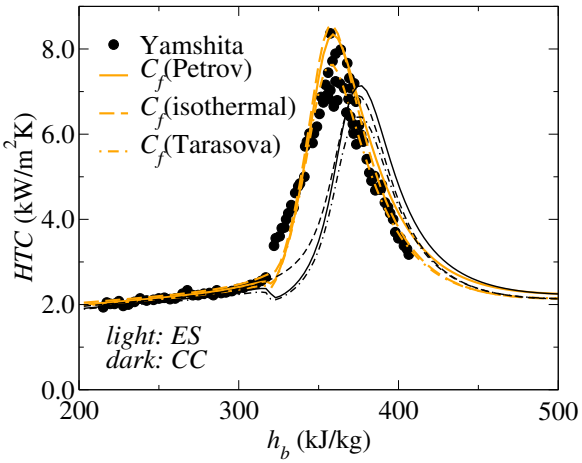


(a) R22 at $p = 5.5$ MPa, $D_h = 4.4$ mm, $G = 1000$ kg/m$^2$s, $q_w = 29.8$ kW/m$^2$.

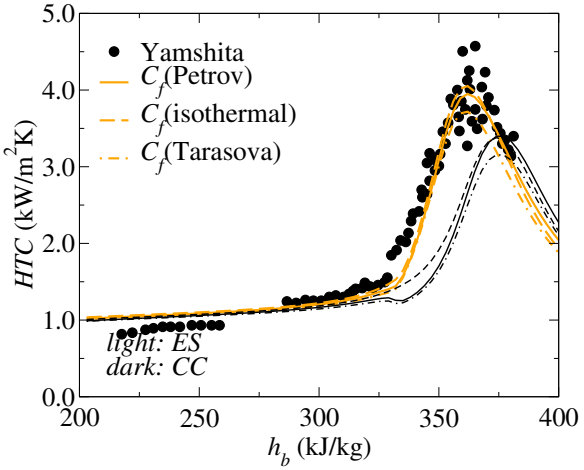


(b) R22 at $p = 5.5$ MPa, $D_h = 4.4$ mm, $G = 400$ kg/m$^2$s, $q_w = 10$ kW/m$^2$.

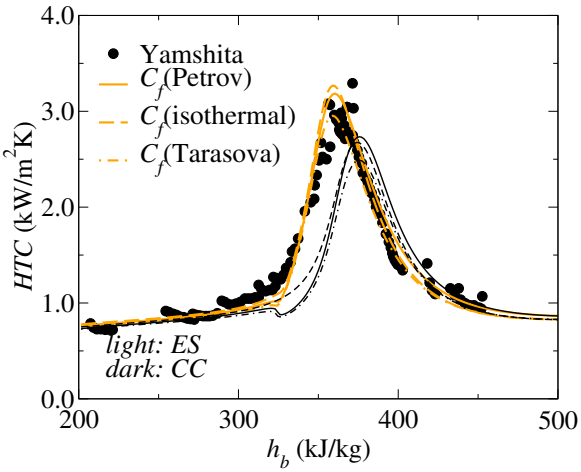


(c) R22 at $p = 5.5$ MPa, $D_h = 13$ mm, $G = 400$ kg/m$^2$s, $q_w = 10.0$ kW/m$^2$

Figure 2: Comparison of the ejection-sweep (orange & thick) & Chilton–Colburn (black & thin) analogies with experimental results by Yamshita et al. 2003.

This shift in the heat transfer coefficient is also clearly visible in the predictions by the ejection-sweep analogy of heat transfer to R134a as shown in figure 3. For all three friction relations, the ejection-sweep analogy outperforms the Chilton–Colburn analogy. However,

unlike the R22-cases, $C_f$(Tarasova) yields attenuated heat transfer coefficients compared to those of the other two skin friction relations, $C_f$(Petrov) and $C_f$(Adiabatic). Even though this is the case, the ejection-sweep yields better predictions than the Chilton–Colburn analogy, which severely underpredicts the experimental heat transfer coefficients in the region $h_b \approx 340 - 400$ kJ/kg and does not predict the location of the heat transfer coefficient correctly.

In the two investigated Helium cases, shown in figure 4, the Chilton–Colburn analogy and the ejection-sweep analogy yield very similar results. This is due to the fact that the difference between the bulk enthalpies and the wall enthalpies are very small, which is the result of the low heat flux. In the $p = 0.3$ MPa case, the ejection-sweep analogy appears to yield slighly better results with respect to the location of the local maximum of the heat transfer coefficient. In the $p = 0.5$ MPa case, the differences between both analogies are negligible.

In the $CO_2$ cases, shown in figure 5, the ejection-sweep analogy yields in conjuction with all three skin friction relations very similar results as before. The predictions of the ejection-sweep formulation are in good agreement with the experimental data by Kim et al. [11] and Kuganov and Kaptil'ny [13]. On the other hand, the Chilton–Colburn relation clearly yields unsatisfactory results for the region $h_b \approx 250 - 350$ kJ/kg.

Figure 6 compares the Chilton–Colburn analogy with the ejection sweep analogy for two different sets of $H_2O$ experimental results. In the case of the experiment by [16], the experimental results are scattered and, therefore, do not reveal a distinct local maximum. In the case of the experiment by [22], the combinaton of the ejection-sweep analogy and $C_f$(Petrov) yields results that are better than the combination of the Chilton–Colburn analogy and the same friction relation. With respect to the other friction relations, neither the ejection-sweep analogy or the Chilton–Colburn analogy is superior. It should be noted that the data sets from [16] and [22] are already close to deterioration (deterioration in water at supercritical pressure has previously been reported to start at $q_w/G \approx 0.4$ [24]).

The performance of the ejection-sweep and Chilton–Colburn analogies was further in-

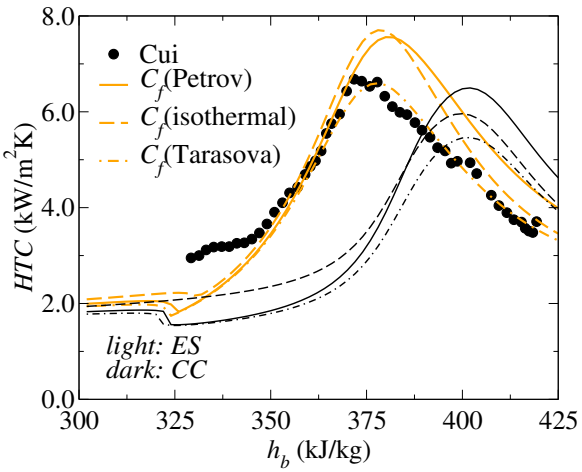


(a) R134a at $p = 4.5$ MPa, $D_h = 8$ mm, $G = 1000$ kg/m$^2$s, $q_w = 40$ kW/m$^2$

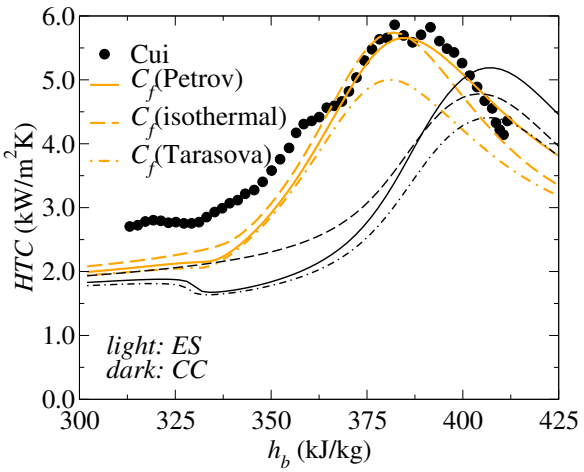


(b) R134a at $p = 4.8$ MPa, $D_h = 8$ mm, $G = 1000$ kg/m$^2$s, $q_w = 40$ kW/m$^2$.

Figure 3: Comparison of the ejection-sweep (orange & thick) & Chilton–Colburn (black & thin) analogies with experimental results by Cui et al. 2018.

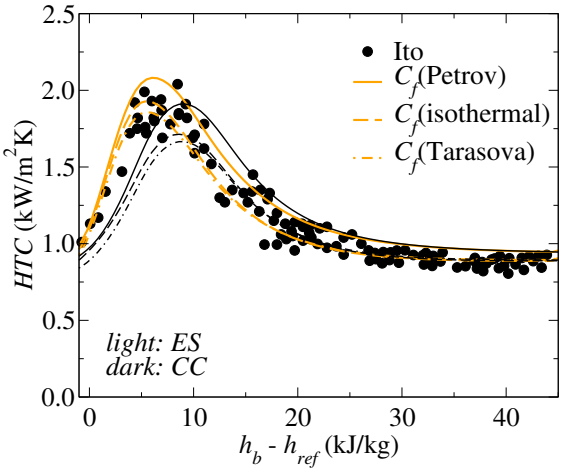


(a) Helium at $p = 0.3$ MPa, $D_h = 1.25$ mm, $G = 40$ kg/m$^2$s, $q_w = 500$ W/m$^2$, $h_{ref} = 5$ kJ/kg.

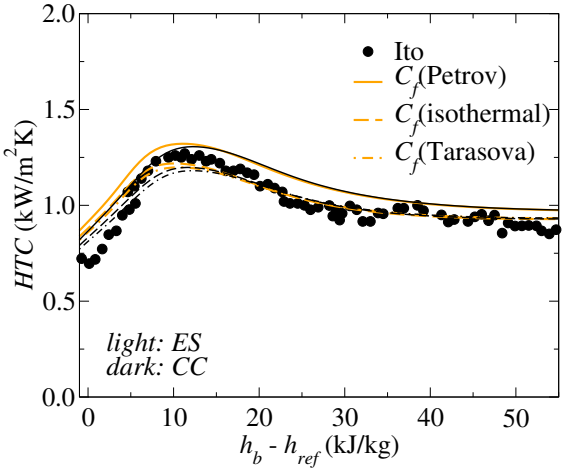


(b) Helium at $p = 0.5$ MPa, $D_h = 1.25$ mm, $G = 40$ kg/m$^2$s, $q_w = 500$ W/m$^2$, $h_{ref} = 5$ kJ/kg.

Figure 4: Comparison of the ejection-sweep (orange & thick) & Chilton–Colburn (black & thin) analogies with experimental results by [6].

vestigated by considering the low heat flux results from [26]; see figure 7. In both cases, the ejection-sweep analogy performs clearly better than the Chilton–Colburn analogy for all three different friction relations.

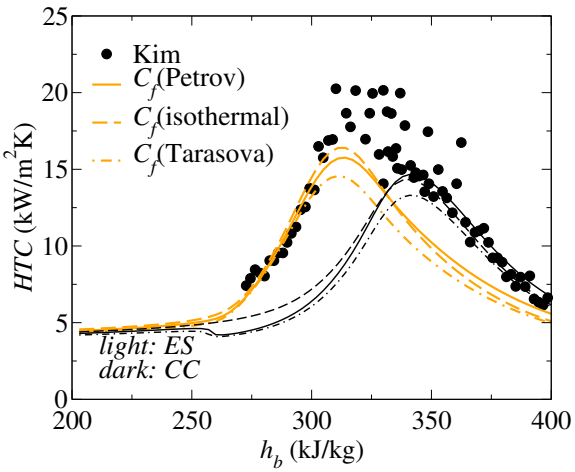


(a) $CO_2$ at $p = 8.12$ MPa, $D_h = 4.4$ mm, $G = 1200$ kg/m$^2$s, $q_w = 50$ kW/m$^2$.

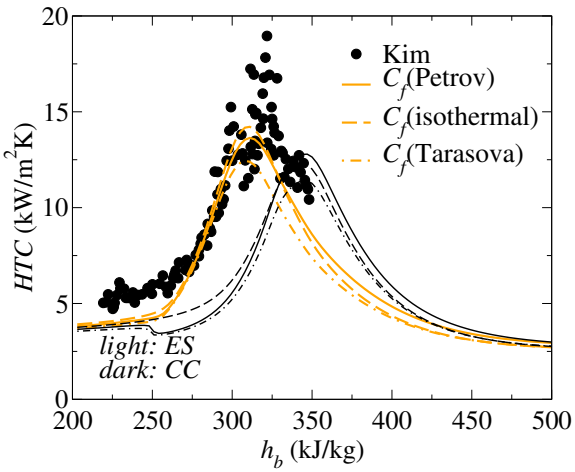


(b) $CO_2$ at $p = 8.12$ MPa, $D_h = 9$ mm, $G = 1200$ kg/m$^2$s, $q_w = 50$ kW/m$^2$.

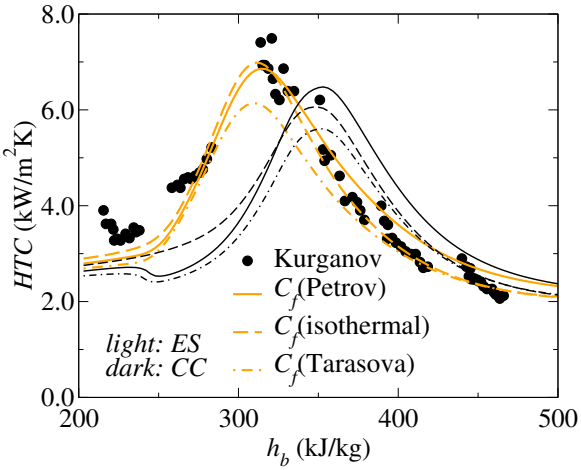


(c) $CO_2$ at $p = 9$ MPa, $D_h = 22.7$ mm, $G = 1036$ kg/m$^2$s, $q_w = 51.8$ kW/m$^2$.

Figure 5: Comparison of the ejection-sweep (orange & thick) & Chilton–Colburn (black & thin) analogies with experimental results by [11] & [13].

### *3.2. Low reduced pressure and medium-high heat flux*

We mentioned earlier in section 2.5 that it is unlikely that the ejection-sweep analogy will work for cases with non-negligible buoyancy and/or acceleration effects. Such effects are much more likely at either lower reduced pressures and for large heat flux to mass flux ratios, as in such condtions large density gradients are to be expected. Figure 8 shows three cases with lower reduced pressures than the cases that were presented up to now. In the case

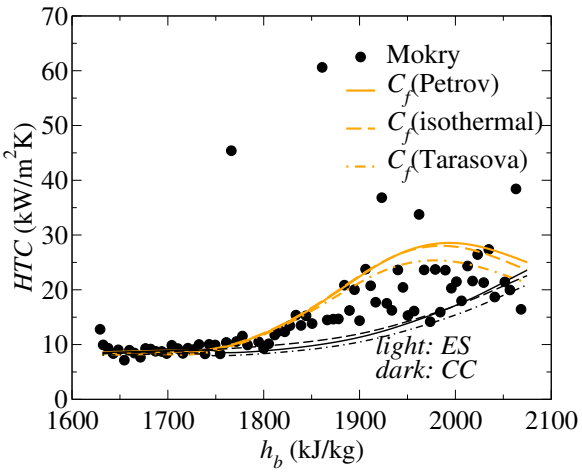


(a) $H_2O$ at $p = 24.5$ MPa, $D_h = 10$ mm, $G = 504$ kg/m$^2$s, $q_w = 141$ kW/m$^2$.

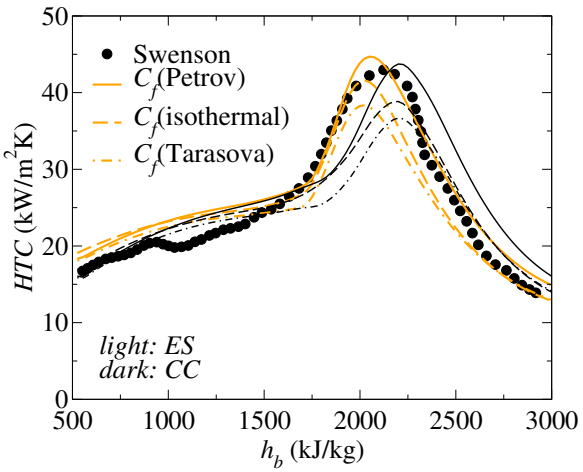


(b) $H_2O$ at $p = 31$ MPa, $D_h = 9.42$ mm, $G = 2149.3$ kg/m$^2$s, $q_w = 787.5$ kW/m$^2$.

Figure 6: Comparison of the ejection-sweep (orange & thick) & Chilton–Colburn (black & thin) analogies with experimental results by [16] and [22].

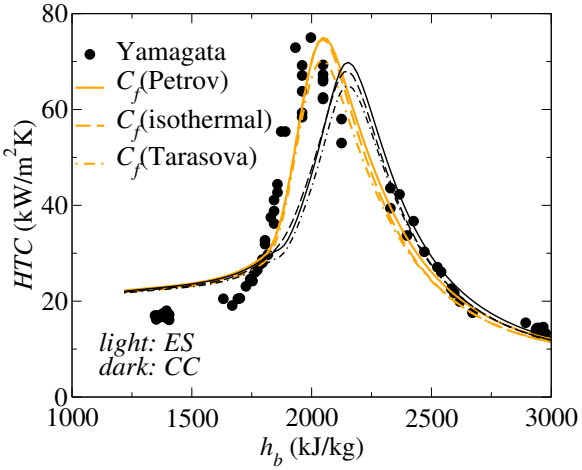


(a) $H_2O$ at $p = 24.5$ MPa, $D_h = 7.5$ mm, $G = 1830$ kg/m$^2$s, $q_w = 233$ kW/m$^2$.

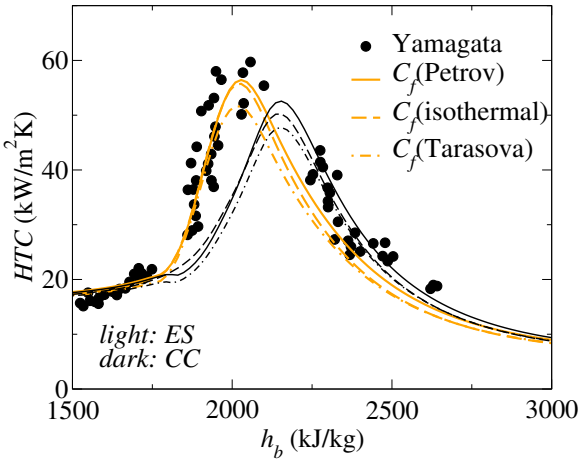


(b) $H_2O$ at $p = 24.5$ MPa, $D_h = 7.5$ mm, $G = 1260$ kg/m$^2$s, $q_w = 233$ kW/m$^2$.

Figure 7: Comparison of the ejection-sweep (orange & thick) & Chilton–Colburn (black & thin) analogies with experimental results by [26].

of R134a, the ejection-sweep analogy predicts the heat transfer coefficient better than the Chilton–Colburn relation does. It is also clear that the difference between the predictions by different friction relations is larger than they were for higher reduced pressures: see figure 3. In the $CO_2$ case, two data sets with different inlet temperatures $T_{in}$ (but otherwise the same

experimental conditions) are compared with the two analogies. The ejection-sweep analogy performs better than the Chilton–Colburn analogy, but only up to $h_b = 325$ kJ/kg. The second heat transfer coefficient peak (present in the set where $T_{in} = 24$ °C) is captured by the Chilton–Colburn relation, but not by the ejection-sweep analogy. Finally, in the $H_2O$ case, neither of the two analogies performs well. These results show that the validity of the ejection-sweep analogy breaks down at pressures (very) close to the critical pressure.

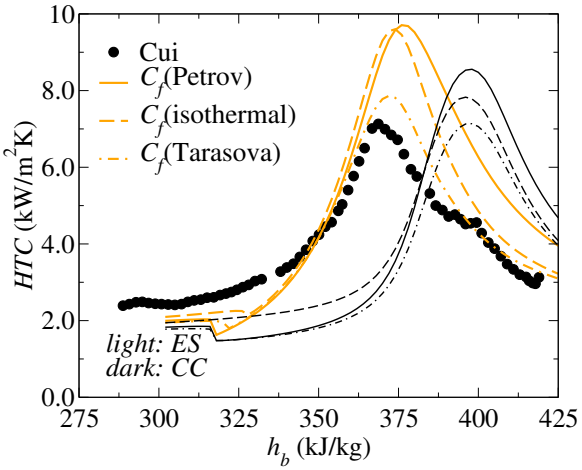


(a) R134a at $p = 4.3$ MPa, $D_h = 8$ mm, $G = 1000$ kg/m$^2$s, $q_w = 40$ kW/m$^2$.

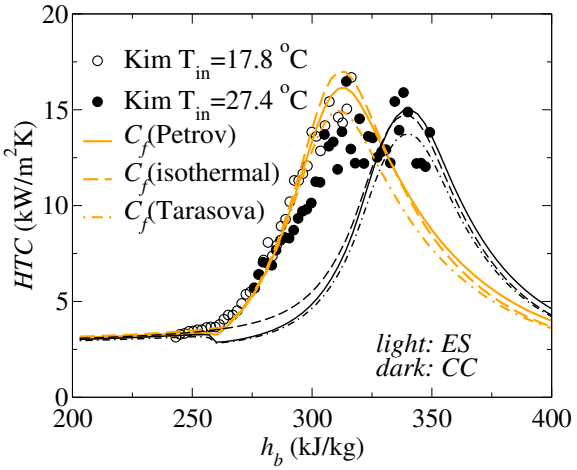


(b) $CO_2$ at $p = 7.75$ MPa, $D_h = 4.4$ mm, $G = 750$ kg/m$^2$s, $q_w = 30$ kW/m$^2$.

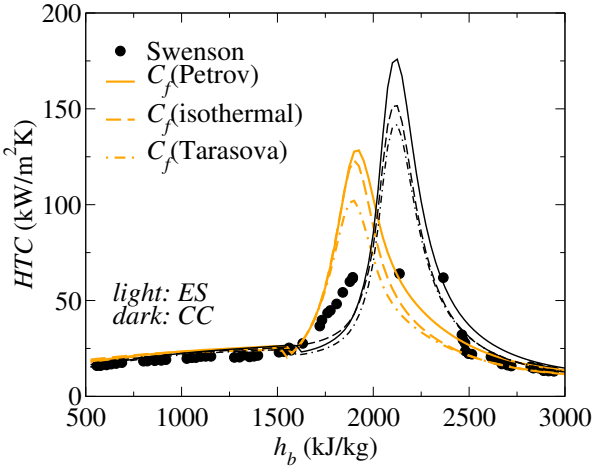


(c) $H_2O$ at $p = 22.8$ MPa, $D_h = 9.42$ mm, $G = 2149.3$ kg/m$^2$s, $q_w = 787.5$ kW/m$^2$.

Figure 8: Comparison of the ejection-sweep (orange & thick) & Chilton–Colburn (black & thin) analogies with experimental results by Cui and Wang [3], Kim et al. [10] and Swenson et al. [22].

In figure 9, we compare both analogies with two comparable experimental cases. In these cases, $q/G$ is higher than 0.4. It is clear here that predictions by both analogies with different friction relations give different results. The combination of the ejection-sweep analogy and $C_f(Petrov)$ yields very good results in both cases. As before, the Chilton–Colburn analogy is not able to predict the location of the maximum heat transfer coefficient with respect to $h_b$ correctly. This is also true for the ejection-sweep analogy in combination with $C_f(Tarasova)$ and $C_f(isothermal)$. These results suggest that the validity of the ejection-sweep correlation breaks down at large heat flux to mass flux ratios.

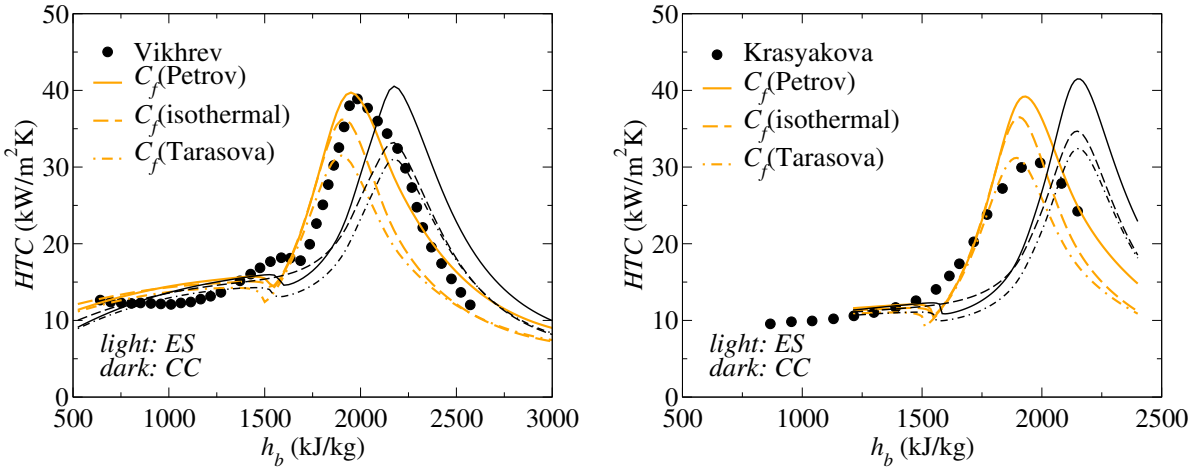


(a) $H_2O$ at $p = 26.5$ MPa, $D_h = 20.4$ mm, $G = 1400$ kg/m$^2$s, $q_w = 700$ kW/m$^2$.

(b) $H_2O$ at $p = 24.5$ MPa, $D_h = 20$ mm, $G = 1000$ kg/m$^2$s, $q_w = 460$ kW/m$^2$.

Figure 9: Comparison of the ejection-sweep (orange & thick) & Chilton–Colburn (black & thin) analogies with experimental results by Vikhrev et al. 1965 and Krasyakova et al. 1967.

### *3.3. Comparisons with literature*

In the previous section, we demonstrated the performance of the ejection-sweep analogy against that of the Chilton–Colburn analogy. Here, we compare the ejection sweep results with two well known correlations from literature. The first was presented by Jackson [7]:

$$Nu = 0.0183 Re_b^{0.82} Pr_b^{0.5} \left(\frac{\rho_w}{\rho_b}\right)^{0.3} \left(\frac{\overline{c_p}}{c_{p,b}}\right)^{p}, \tag{20}$$

where the coefficient $n$ is determined as:

$$p = \begin{cases} 0.4 & \text{if } T_b < T_w < T_{pc} \text{ or } 1.2T_{pc} < T_b < T_w \\ 0.4 + 0.2(T_w/T_{pc} - 1) & \text{if } T_b < T_{pc} < T_w \\ 0.4 + 0.2(T_w/T_{pc} - 1)\left[1 - 5(T_b/T_{pc} - 1)\right] & \text{if } T_{pc} < T_b < 1.2 \text{ and } T_b < T_w, \end{cases} \tag{21}$$

where $T_{pc}$ is the pseudo-critical temperature; the temperature for which the specific heat capacity has a maximum value. The second relation was developed by Mokry et al. [16] and reads:

$$Nu_b = 0.0061 Re_b^{0.904} \overline{Pr}^{0.684} \left(\frac{\rho_w}{\rho_b}\right)^{0.564} \tag{22}$$

It should be noted that equation (22) was not specifically developed for different fluids, while equation (20) was developed for only $CO_2$ and water. Predictions by equations (20 and (22) were compared to those of the ejection-sweep analogy for the Helium, refrigerants, $CO_2$ and water cases. We present the results for four representitative different cases in figure (10). For the heated Helium case, equation (22) severely underpredicts the experimental results, while equation (20) only slightly underpredicts the data. In the R134a case, the trend of the heat transfer coefficient is generally well captured by the ejection-sweep analogy, but not by equations (20) and (22); both equations severely underpredict the heat transfer coefficient in the region $h_b = 360 - 380$ kJ/kg. There is a similar difference between equation (20) and the experimental results in the $CO_2$ case. However, in the same case, equation (22) yields very similar (if not slightly overpredictive) results as the experimental & ejection-sweep analogy results. Finally, in the water case, both equations (20) and (22) as well as the ejection-sweep analogy perform very well, though equation (22) yields slightly over-predicted results and the location of the heat transfer coefficient peak is not entirely correctly predicted by equation (20). The results in figure 10 show that the ejection-sweep analogy is better at predicting heat transfer for different fluids at supercritical fluids than equations 22 and 20 at low heat flux to mass flux ratios.

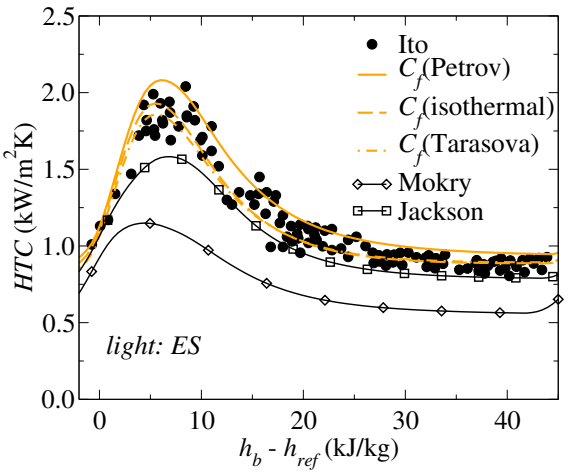


(a) Helium at $p = 0.3$ MPa, $D_h = 1.25$ mm, $G = 40$ kg/m$^2$s, $q_w = 500$ W/m$^2$.

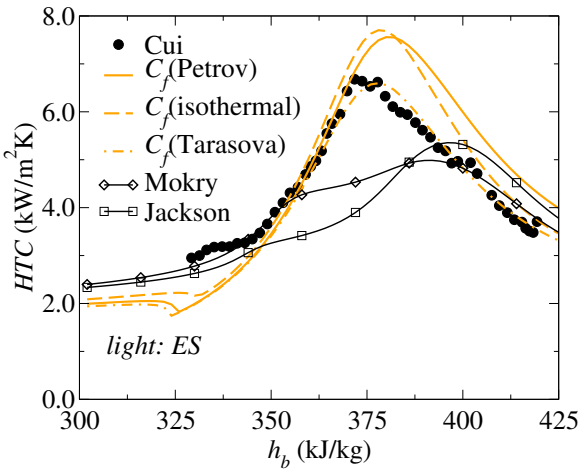


(b) R134a at $p = 4.5$ MPa, $D_h = 8$ mm, $G = 1000$ kg/m$^2$s, $q_w = 40$ kW/m$^2$.

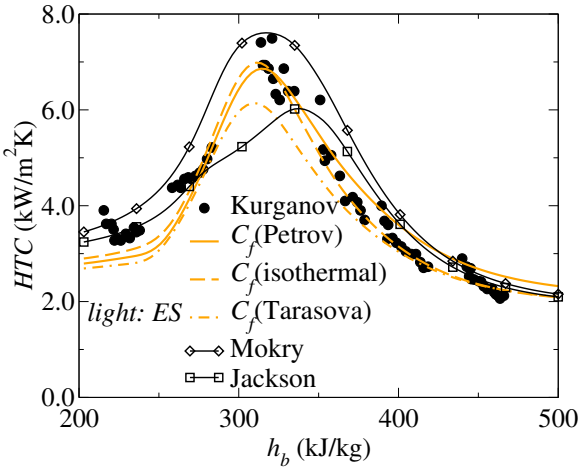


(c) $CO_2$ at $p = 9$ MPa, $D_h = 22.7$ mm, $G = 1036$ kg/m$^2$s, $q_w = 51.8$ kW/m$^2$.

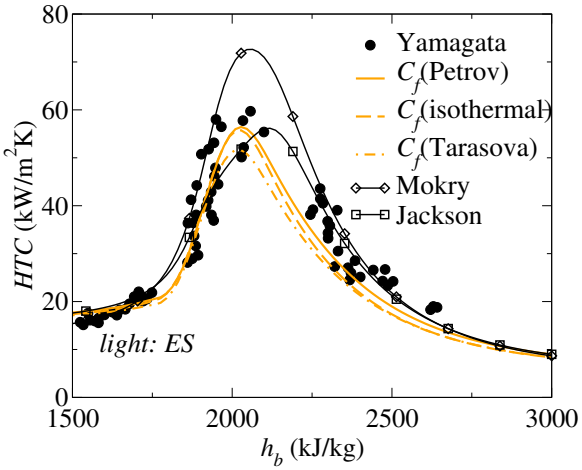


(d) $H_2O$ at $p = 24.5$ MPa, $D_h = 7.5$ mm, $G = 1260$ kg/m$^2$s, $q_w = 233$ kW/m$^2$.

Figure 10: Comparison of the ejection-sweep analogy and relations developed by Mokry et al. [16] and Jackson [7].

## 4. Discussion

A new friction-heat transfer analogy, based on small scale physical phenomena, was derived in order to model heat transfer to turbulent fluids at supercritical pressure. Predictions of the new analogy, named ejection-sweep analogy, were compared to different experimental results alongside predictions of the Chilton–Colburn analogy. Both analogies were used in conjunction with three different skin friction relations.

It was found that the ejection-sweep analogy yields excellent predictions with respect to experimental cases where the heat flux to mass flux ratio is small or where buoyancy and acceleration effects are negligible. It was shown that the ejection-sweep analogy performs well for five different fluids at supercritical pressure: refrigerants R22 and R134a, $CO_2$, Helium and $H_2O$. In all cases, but the Helium cases, the predictions of the ejection-sweep was shown to be superior to that of the Chilton–Colburn relation.

At conditions that are close to deterioration, or at medium high heat flux to mass flux ratios, it is clear that the ejection-sweep analogy performs less well with respect to experimental results. Only in combination with one skin friction relation was it shown that the ejection-sweep analogy is superior to the Chilton–Colburn analogy.

The ejection-sweep analogy was also compared to two well known relations from literature. It was shown that both these relations as well as the ejection-sweep analogy performs very well in the investigated supercritical water cases. However, for the $CO_2$, helium and refrigerant cases, the ejection sweep analogy performed better. Especially in the R134a and Helium cases, the ejection-sweep analogy outperformed the relations from literature.

This work shows that the newly devised ejection-sweep analogy does not solve the problem of heat transfer to fluids at supercritical pressure for all possible conditions (especially for deteriorated heat transfer conditions). However, as it performs well for different fluids and at low heat transfer to mass flux ratios, it may find use in new heat transfer relations that are of the form $Nu/Nu_{ES} = \mathcal{G}(Bo, Ac, ...)$, where $G$ is a function and $Bo$ and $Ac$ denote non-dimensional groups that represent the effects of buoyancy and thermal acceleration, resepctively. In other words, the ratio $Nu/Nu_{ES}$ may help to identify a general description or relation for the heat transfer to supercritical fluids in deteriorated regimes.

## References

[1] G.N. Abramovich. *The theory of turbulent jets.* Massachusetts Insitute of Technology, Cambridge, MA, 1963.

[2] R.F. Blackwelder and J.H. Haritonidis. Scaling of the bursting frequency in turbulent boundary layers. *Journal of Fluid Mechanics*, 132:87–103, 1983.

[3] Y.-L. Cui and H.-X. Wang. Experimental study on convection heat transfer of r134a at supercritical pressures in a vertical tube for upward and downward flows. *Applied Thermal Engineering*, 129:1414–1425, 2018.

[4] G. Hetsroni, L.P. Yarin, and D. Kaftori. A mechanistic model for heat transfer from a wall to a fluid. *International Journal of Heat and Mass Transfer*, 39:1475–1478, 1996.

[5] X. L. Huai, S. Koyama, and T. S. Zhao. An experimental study of flowand heat transfer of supercritical carbon dioxide in multi-port mini channels under cooling conditions. *Chemical engineering science*, 60:3337–3345, 2005.

[6] T. Ito, D. Kasao, M. Yamaguchi, H. Mori, and T. Hara. Forced convective heat transfer to supercritical helium. *Journal of Cryogenics and Superconductivity Society of Japan*, 21:327–333, 1986.

[7] J. D. Jackson. Consideration of the heat transfer properties of supercritical pressure water in connection with the cooling of advanced nuclear reactors. *Proceedings of the 13th Pacific Basin Nuclear Conference, Shenzen City, China, October 21-25.*, 2002.

[8] J.D. Jackson. Fluid flow and convective heat transfer to fluids at supercritical pressure. *Nuclear Engineering and Design*, 264:24–40, 2013.

[9] J.D. Jackson. Models of heat transfer to fluids at supercritical pressure with influences of buoyancy and acceleration. *Applied Thermal Engineering*, 124:1481–1491, 2017.

[10] H. Kim, Y.-Y. Bae, H.-Y. Kim, J. Song, and B.-H. Cho. Experimental investigation of the heat transfer characteristics in upward flow of supercritical carbon dioxide. *Nuclear Technology*, 164:119–129, 2008.

[11] H. Kim, H. Y. Kim, J. H. Song, and Y. Y. Bae. Heat transfer to supercritical pressure carbon dioxide flowing upward through tubes and a narrow annulus passage. *Progress in Nuclear Energy*, 50:518–525, 2008.

[12] L.Y. Krasyakova, I. I. Belyakov, and N. D. Fefelova. Heat transfer with a downward flow of water at supercritical pressure. *Thermal Engineering*, 24:9–14, 1977.

[13] V. A. Kuganov and A. G. Kaptil'ny. Velocity and enthalpy fields and eddy diffusivities in a heated supercritical fluid flow. *Experimental Thermal and Fluid Science*, 5:465–478, 1992.

[14] H. Li, Y. Zhang, M. Yao, Y. Wang, H. Wangand Y. Yang, and W. Guo. An improved modeling on convection heat transfer of supercritical fluids for several advanced energy systems. *International journal of heat and mass transfer*, 111:771–781, 2017.

[15] S.-H. Lio, Y.-P. Huang, J.-F. Wang G.-X. Liu, and L. K. H. Leung. A predictive–corrective process for predicting forced convective heat trasnfer in heated tubes at supercritical pressure. *International journal of heat and mass transfer*, 110:374–382, 2017.

[16] S. Mokry, I. Pioro, A. Farah, K. King, S. Gupta, W. Peiman, and P. Kirillov. Development of supercritical water heat-transfer correlation for vertical bare tubes. *Nuclear Engineering and Design*, 241:1126–1136, 2011.

[17] S. Pandey and E. Laurien. Heat transfer analysis at supercritical pressure using two layer theory. *The Journal of Supercritical Fluids*, 109:80 – 86, 2016.

[18] J. W. R. Peeters, R. Pecnik, M. Rohde, T. H. J. J. van der Hagen, and B. J. Boersma. Characteristics of turbulent heat transfer in an annulus at supercritical pressure. *Physical review fluids*, 2:024602, 2017.

[19] N.E. Petrov and V.N. Popov. Heat transfer and hydraulic resistance with turbulent flow in a tube of water under supercritical parameters of state. *Thermal Engineering*, 35:577–580, 1988.

[20] B. S. Petukhov, V. A. Kurganov, and V. B. Ancudinov. *Teplofiz. Vys. Temp.*, 21, 1983.

[21] I. L. Pioro, R. B. Duffey, and T. J. Dumouchel. Hydraulic resistance of fluids flowing in channels at supercritical pressures (survey). *Nuclear Engineering and Design*, 231: 187–197, 2004.

[22] H. S. Swenson, J. R. Carver, and C. R. Kakarala. Heat transfer to supercritical water in smooth-bore tubes. *Journal of Heat Transfer*, 87:477–484, 1965.

[23] N. V. Tarasova and A. I. Leont'ev. Hydraulic resistance during flow of water in heated pipes at supercritical pressures. *High Temperatures*, 6:721–722, 1968.

[24] Y. V. Vikhrev, Y. D. Barulin, and A. S. Kon'kov. Hydraulic resistance during flow of water in heated pipes at supercritical pressures. *Thermal Engineering*, 14:116–119, 1967.

[25] W. Wang, D. Yang, M. Qu H. Jiang, and Y. Zhao. Heat transfer and frictional resistance characteristics of the water wall tube of an ultra-supercritical cfb boiler. *The Journal of Supercritical Fluids*, 128:279–290, 2017.

[26] K. Yamagata, K. Nishikawa, S. Hasegawa, T. Fujii, and S. Yoshida. Forced convective heat transfer to supercritical water flowing in tubes. *International Journal of Heat and Mass Transfer*, 15:2575–2593, 1972.

[27] T. Yamashita, S. Yoshida, H. Mori, S. Morooka, H. Komita, and K. Nishida. Paper 1119: Heat transfer study under supercritical pressure conditions. *GENES4/ANP2003, Sep. 15-19, 2003, Kyoto, JAPAN*, 2003.

[28] J.Y. Yoo. The turbulent flows of supercritical fluids with heat transfer. *Annual Review of Fluid Mechanics*, 45(1):495–525, 2013.

[29] C.-R. Zhao and P.-X. Jiang. Experimental study of in-tube cooling heat transfer and pressure drop characteristics of r134a at supercritical pressures. *Experimental thermal and fluid science*, 35:1293–1303, 2011.